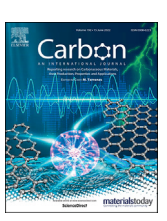


Contents lists available at ScienceDirect

Carbon





Phenylenediamine-derived near infrared carbon dots: The kilogramscale preparation, formation process, photoluminescence tuning mechanism and application as red phosphors



Chunyu Ji ^{a, b, 1}, Qiurui Han ^{a, 1}, Yiqun Zhou ^c, Jiajia Wu ^a, Wenquan Shi ^a, Lipeng Gao ^a, Roger M. Leblanc ^c, Zhili Peng ^{a, b, *}

- ^a School of Materials and Energy, Yunnan University, Kunming, 650091, PR China
- ^b Advanced Computing Center, Materials Genome Institute, Yunnan University, Kunming, 650091, PR China
- ^c Department of Chemistry, University of Miami, 1301 Memorial Drive, Coral Gables, Florida, 33146, USA

ARTICLE INFO

Article history: Received 3 January 2022 Received in revised form 19 February 2022 Accepted 25 February 2022 Available online 28 February 2022

Keywords:
Kilogram-scale
Near-infrared carbon dots
2
3-Diaminophenazine
Photoluminescence tuning
Surface state
Red phosphors

ABSTRACT

Kilogram-scale preparation of near infrared (NIR) carbon dots (C-dots) from *o*-phenylenediamine (*o*-PDA) with over 96% yield was reported in this study, and the estimated cost for each gram of C-dots was only \$ 0.1. The formation process of the C-dots was elucidated and the structural model was also proposed in which the key intermediates were revealed. Excitingly, the optical properties of the C-dots could be reversibly tuned *via* a facile protonation-deprotonation process. Upon protonation, fluorescence emission wavelength of the C-dots could be red shifted for 47 nm, and deprotonation could enhance the photoluminescence quantum yield by three times. These optical alterations were attributed to stabilization of the excited electrons by the surface protons, and diagrams showing the electronic transition states of the C-dots were proposed according to the calculated band gaps. The as prepared C-dots demonstrated themselves as cheap and readily available phosphors for the assembling of red LEDs.

 $\ensuremath{\texttt{©}}$ 2022 Elsevier Ltd. All rights reserved.

1. Introduction

As a new type of zero-dimensional carbon-based nanomaterials, carbon dots (C-dots) were serendipitously discovered back in 2004 and attracted continuous attention since 2006 [1,2]. Thanks to their superior properties, C-dots have been widely applied in bioimaging, drug delivery, sensing, catalysis, anti-counterfeiting, photovoltaic devices and other fields [3–8]. With the continuous efforts from scientists all over the world in the past 15 years, numerous obstacles have been conquered during the development of C-dots, which significantly promoted the advancements and expanded applications of C-dots. For instance, the synthesis of C-dots was quite difficult in the early days, which mainly included laser burning [9,10], oxidative acid treatment [11,12], electrochemical peeling

[13], etc. These methods were not only complicated to carry out but also require tedious post-processing. With the prevailing of bottom-up synthesis methods (i.e., hydrothermal, solvothermal, microwave treatment and direct heating, etc.) later on, the preparation of C-dots has become much facile and versatile [14]. Similarly, most of C-dots were blue, green emissive in the early days, red or near-infrared (NIR) emissive C-dots that are essential for biomedical applications and optoelectronic devices fabrication were rare. Excitingly, researchers have constructed series of NIR Cdots from cheap carbon precursors (i.e., citric acid [15–18], aniline [19-21], phenol [22-24], polythiophene [25-27], and biomass [28,29]) in recent years, which greatly promoted the further development of C-dots. Furthermore, the understanding towards the intrinsic nature, structure and photoluminescence (PL) mechanism of C-dots in the early days was rather limited. Luckily, our understandings towards these issues have been much advanced [30-34], which significantly accelerated the rational design and application of C-dots.

Despite the above-mentioned advancements, there are still some key issues waiting to be addressed. Firstly, the lack of reliable,

^{*} Corresponding author. School of Materials and Energy, Yunnan University, Kunming, 650091, PR China.

E-mail address: zhilip@ynu.edu.cn (Z. Peng).

¹ These authors contributed equally to this work.

reproducible and economic large-scale synthesis of C-dots significantly lagged behind their superior properties, limiting their practical applications and commercialization. Up till now, only a few groups reported large-scale synthesis of C-dots [29,35,36] (Table S1), and these studies were generally suffered from low yields and lacking of proper purification methods. Furthermore, most large-scale synthesized C-dots emit only blue, green light, red-emitting C-dots in gram-scale was rather rare [37]. Secondly, Cdots currently are either used without purification or treated with dialysis, column chromatography, etc., which hardly meet the requirements for C-dots isolation and purification once the production of C-dots are scaled up for commercialization purpose. Lastly, common practices for tuning C-dots emission wavelength and enhancing their quantum yields (QYs) include carbon precursor selection [19], heteroatom doping [38], surface modification [39] as well as C-dots size regulation [40]. However, these approaches generally require complicated operations and sometimes have very limited tuning capabilities. As such, the ability to synthesize NIR Cdots in large scale (i.e., kilogram-scale) with facile purification process and easy PL tuning is still hard to achieve and highly desired.

In this context, to the best of our knowledge, we report for the first time the kilogram-scale synthesis of NIR C-dots with facile purification and convenient but effective PL tuning. Specifically, kilogram-scale NIR C-dots were prepared from o-phenylenediamine (o-PDA) via a combinative of microwave-hydrothermal treatment, and the resulted C-dots could be facilely purified by simple filtering after pH adjustment. The overall yield of C-dots is 96% and the estimated cost to produce each gram of C-dots is only about \$ 0.1. Excitingly, the PL of the obtained C-dots could be conveniently tuned via a straightforward protonation and deprotonation process: protonation could result a significant red shift (47 nm) of the emission wavelength of the samples while deprotonation could greatly enhance the fluorescence QYs (3 times). Last, the kilogram-scale NIR C-dots demonstrated high potential as red LED phosphors.

2. Materials and methods

2.1. Reagents and materials

Sodium hydroxide (NaOH 96%), hydrochloric acid (HCl 36%—38%) and sulfuric acid (H₂SO₄ 95%—98%) were purchased from Chengdu chron chemicais company. *O*-phenylenediamine (*o*-PDA) (98%), *tert*-butyl hydroperoxide (TBHP) (70%), 3-chloroperbenzoic acid (85%), N, N-Diisopropylethylamine (98%) and 8-Diazabicyclo [5.4.0] undec-7-ene (99%) were purchased from Energy Chemical Company. All the reagents were used as received without further purification, unless otherwise noted. The deionized water used in all experiments was made from a Master Touch-S laboratory ultrapure water machine (Master Touch, Shanghai, People's Republic of China).

2.2. Synthesis of C-dots

C-dots $_{568}$: a mixture of o-PDA (0.25 g) and deionized water (20 mL) was heated in a microwave synthesizer set at 150 °C for 20 min. After the reactor was cooled to room temperature, the resulted solution was freezing dried to obtain a yellow solid powder.

C-dots $_{626}$: a mixture of o-PDA (0.25 g), HCl (2 mL), TBHP (0.2 mL) and deionized water (20 mL) was heated in a microwave synthesizer set at 150 °C for 20 min. After the reactor was cooled to room temperature, the resulted solution was freezing dried to obtain a brownish solid powder that was not stable in their solid state.

C-dots $_{653}$ synthesized with microwave synthesizer: a mixture of o-PDA (0.25 g), HCl (2 mL), TBHP (0.2 mL) and deionized water (20 mL) was heated in a microwave synthesizer set at 150 °C for 20 min. After the reactor was cooled to room temperature, the mixed solution was transferred to an autoclave and heated at 200 °C for 12 h. Then the autoclave was cooled down to room temperature, the reaction mixture was filtered, and the residues were washed with water. Finally, they were collected and vacuum dried to result the product as black powders.

C-dots₆₅₃ synthesized with domestic microwave: a mixture of o-PDA (0.25 g), HCl (2 mL), TBHP (0.2 mL) and deionized water (20 mL) was heated in a domestic microwave set at 200 W for 20 min. After the reactor was cooled to room temperature, the mixed solution was transferred to an autoclave and heated at 200 °C for 12 h. Then the autoclave was cooled down to room temperature, the reaction mixture was filtered, and the residues were washed with water. Finally, they were collected and vacuum dried to result the product as black powders.

C-dots₆₀₆ synthesized with domestic microwave: a mixture of o-PDA (0.25 g), H_2SO_4 (2 mL), 3-chloroperbenzoic acid (0.2 g) and deionized water (20 mL) was heated in a domestic microwave set at 200 W for 20 min. After the reactor was cooled to room temperature, the mixed solution was transferred to an autoclave and heated at 200 °C for 12 h. After the reactor was cooled to room temperature, the mixed solution was transferred to an autoclave and heated at 200 °C for 12 h. Then the autoclave was cooled down to room temperature, and the resulted solution was adjusted to be neutral with diluted NaOH solution before they were filtered. The residues were washed with water, collected and vacuum dried to result the desired product as black powders.

C-dots₆₀₆ synthesized with domestic microwave in kilogram-scale: a mixture of o-PDA (1.15 kg), 3-Chloroperbenzoic acid (57.5 g), H₂SO₄ (575 mL), and deionized water (2500 mL) was heated in a household microwave at 200 W for 20 min. After the reactor was cooled to room temperature, the mixed solution was transferred to an autoclave and heated at 200 °C for 12 h. Then the autoclave was cooled down to room temperature, and the resulted solution was adjusted to be neutral with diluted NaOH solution before they were filtered. The residues were washed with water, collected and vacuum dried to result the desired product as black powders.

2.3. Characterizations of C-dots

The absorption spectrum of the methanol solution of C-dots (1 $\mu g/mL)$ was detected by an ultraviolet—visible spectrophotometer (UV—vis, UV-2600, Shimadzu, Japan). Put 3 mL of methanol in two 1 \times 1 \times 3 cm cuvettes, and then put the cuvettes in the UV—vis base to test the solvent baseline. The wavelength range is 195—700 nm, the scanning speed is medium speed, the sampling interval is 1 nm, and the sampling times are repeated twice. Add 3 mL of C-dots solution to a 1 \times 1 \times 3 cm cuvette, and then place it in the UV—vis base to test the absorption spectrum.

The fluorescence spectrum of C-dots (10 μ g/mL) was tested by a fluorescence spectrometer (FL, F97 Pro, Shanghai Prism Technology Co., Ltd.). Add 3 mL of C-dots solution to a 1 \times 1 \times 3 cm cuvette to test the fluorescence spectrum. The scanning method is three-dimensional wavelength scanning. The excitation wavelength is 260–580 nm, and the excitation width is 10 nm. The emission wavelength is 500–850 nm, and the emission width is 10 nm. The scanning speed is 3000 nm/min, and the scanning interval is 1 nm. The gain is 650 V.

The infrared absorption spectrum of the C-dots was measured by a Fourier Infrared Spectrometer (FTIR, Middle Age Walker, Thermo, USA) with a resolution of 4 cm. Put 300 mg of potassium

bromide in an agate mortar, fully dry it at $80\,^{\circ}\text{C}$ (6 h), add 2 mg of C-dots and grind thoroughly. Then dry at $80\,^{\circ}\text{C}$ for 5 min, and then continue to grind for 30 s. Put the ground powder into a mold and press a 10 t press. Put the pressed sample into FTIR to test the infrared absorption spectrum.

The surface charge at C-dots was tested by a Zeta potential analyzer (Zeta potential, sample cell DTS1060, Malvern, UK). The particle size of C-dots was measured by transmission electron microscope (TEM, JEM-2100, US FEI). The acceleration voltage is 200 kV, and the magnification is 300,000 times. The elemental composition of C-dots was tested by multifunctional X-ray photoelectron spectroscopy (XPS, K-Alpha, Thermo, USA). The Raman spectra of the C-dots were tested by a micro confocal Raman spectrometer (Raman, inVia, Renishawin, UK).

Dissolve the C-dots solid powder in methanol solution to prepare a 10 μ g/mL C-dots solution. Filter the prepared C-dots solution with a 0.22 μ m organic filter membrane. The filtered solution was put into a 1.5 mL glass bottle dedicated to the mass spectrometer and the relative molecular mass of the C-dots was measured by the mass spectrometer.

2.4. Preparation of red phosphors and construction of LED devices

First, the C-dots (10 mg) and polyvinylpyrrolidone (K10–K14, 500 mg) were dissolved in ethanol (40 mL) to form a mixed solution. Then, the mixed solution was dried on a constant temperature drying table (50 °C). The resulted material was ground in an agate mortar and sieved through a mesh sieve to obtain fine C-dots phosphors. UV-LED chips (LUMEX-SSL-LXTO46UV1C) with the peak emission wavelength centered at 382 nm were used for red LED fabrication. A certain amount of red phosphor was coated on the surface of the LED chip to construct a red LED device.

3. Results and discussion

3.1. Synthesis optimization of C-dots

3.1.1. Synthesis method

The desired C-dots in this study were synthesized from o-PDA in an acidic (HCl) and oxidative (TBHP) environment, which was first treated by microwave synthesizer at 150 °C for 20 min, followed immediately by hydrothermal treatment at 200 °C for 12 h. It is worth noting that treatment of o-PDA with only microwave irradiation resulted in yellow C-dots that emitted at 568 nm (noted as C-dots₅₆₈, Fig. 1a). Since C-dots₅₆₈ did not achieve red or NIR luminescence, which we attributed to that the degree of polymerization of the carbon source (o-PDA) was too low, thus we added HCl and TBHP to our reaction in the hope to activate the amino groups of o-PDA and increase the degree of polymerization. To our delight, with the inclusion of the two reagents, NIR C-dots that emit at 626 nm was successfully obtained (noted as C-dots₆₂₆, Fig. 1b). However, the sample was unstable and subject to quick deterioration, which we attributed to the insufficient carbonization with only microwave irradiation. As such, the sample after microwave irradiation was further processed by hydrothermal treatment (200 °C, 12 h) in the hope to increase the degree of carbonization, which successfully resulted in stable NIR C-dots that emitted at 653 nm (noted as C-dots₆₅₃, Fig. 1c) with 86% yield (Table 1, row 3).

3.1.2. Synthesis reagent

It's worth noting, it's important to keep an acidic and oxidative reaction environment to obtain the targeted C-dots: our control experiment showed that if the reaction was run without HCl, C-dots₆₅₃ could not be produced (Fig. 1d); Similarly, when the reaction proceeded without TBHP, C-dots₆₅₃ could still be generated

(Fig. 1e), however, with a significantly decreased yield (23%, Table 1, **row 5**). In addition to the reagents, our control experiments also showed that pre-treatment by microwave irradiation before hydrothermal reaction is essential for the successful production of the NIR C-dots: C-dots₆₅₃ could still be generated subjected to a direct hydrothermal reaction without the microwave treatment. However, the yield was greatly reduced (46%, Table 1, **row 6**), and a large amount of impurities were inevitably produced (Fig. 1f).

3.1.3. Large-scale preparation

The microwave synthesizer can only process 0.25 g of o-PDA at a time, which is far insufficient for large-scale synthesis of C-dots. Therefore, the microwave synthesizer was replaced by a domestic microwave oven for the pretreatment to test the possibility of scaling up the reaction. Unfortunately, under identical reaction conditions with the domestic microwave oven, the yield of C-dots₆₅₃ were greatly reduced (34%, Table 1, row 7), which might be attributed to the reason that significant amount of HCl and TBHP was lost because of their high volatility in an open-air reaction. As such, the two chemicals HCl and TBHP were replaced with their less volatile counterparts H₂SO₄ and 3-chloroperbenzoic acid (m-CPBA), respectively. Our experiments showed that substitutions of HCl with H₂SO₄ and TBHP with m-CPBA had no obvious effect on the optical properties of C-dots₆₅₃ (Figs. S1 and S2), while increased their yields greatly (Table 1, row 8). To our delight, the yield of the C-dots was significantly enhanced by adjusting the pH of the reaction mixtures to neutral before post-processing (94%, Table 1, row 9); it's worth to mention, the best emission of the C-dots obtained also shifted to 606 nm (noted as C-dots₆₀₆, Fig. 2c), which we will discuss carefully later on. With these optimizations, the reaction was successfully carried out on a kilogram-scale that could produce C-dots₆₀₆ with almost quantitative yield (96%, Table 1, row 10) at an extremely low cost (about \$ 0.1 for each gram of C-dots, see Table S2).

Based on the above discussions, the formation of C-dots could be reasonably summarized as: under acidic environment, microwave irradiations provide sufficient energy to initiate the orderly polymerization of *o*-PDA; following that, the hydrothermal treatment could further prompt the polymerization process and complete the carbonization step to generate C-dots with the help of oxidative reagent. In the reaction, the amino groups were multi functional. Firstly, they provided active sites for the polymerization process to occur and expand; secondly, they become part of the surface functionalities of the finalized C-dots; lastly, the amino groups also provided sufficient amount of nitrogen doping for the finalized C-dots and became part of the skeleton of the carbonized core. Various studies have shown that doping with nitrogen atoms could greatly enhance the fluorescence QYs of C-dots [38].

3.2. Characterization and analysis

To analyze the morphological, optical, chemical and structural properties of the as prepared C-dots (*C*-dots₆₀₆), characterizations by TEM microscopy, UV—vis and fluorescence, FTIR and XPS, XRD and Raman spectroscopy, as well as zeta potential were performed. TEM microscopy was first applied to explore the morphologies and structural characteristics of the sample. As can be seen (Fig. 2a), C-dots₆₀₆ are well dispersed spherical particles with no obvious agglomerates, which might be attributed to their negatively charged surfaces as indicated by their zeta potential (–12.5 mV). There are no obvious lattice structures for these particles, indicating that they probably have amorphous cores. In general, the diameters of these particles range from 1.8 to 3.7 nm, with an average diameter of 2.8 nm (Fig. 2b).

Next, we studied the spectroscopic behaviors of C-dots₆₀₆. The ethanol solution of C-dots₆₀₆ was pink under ambient light, and

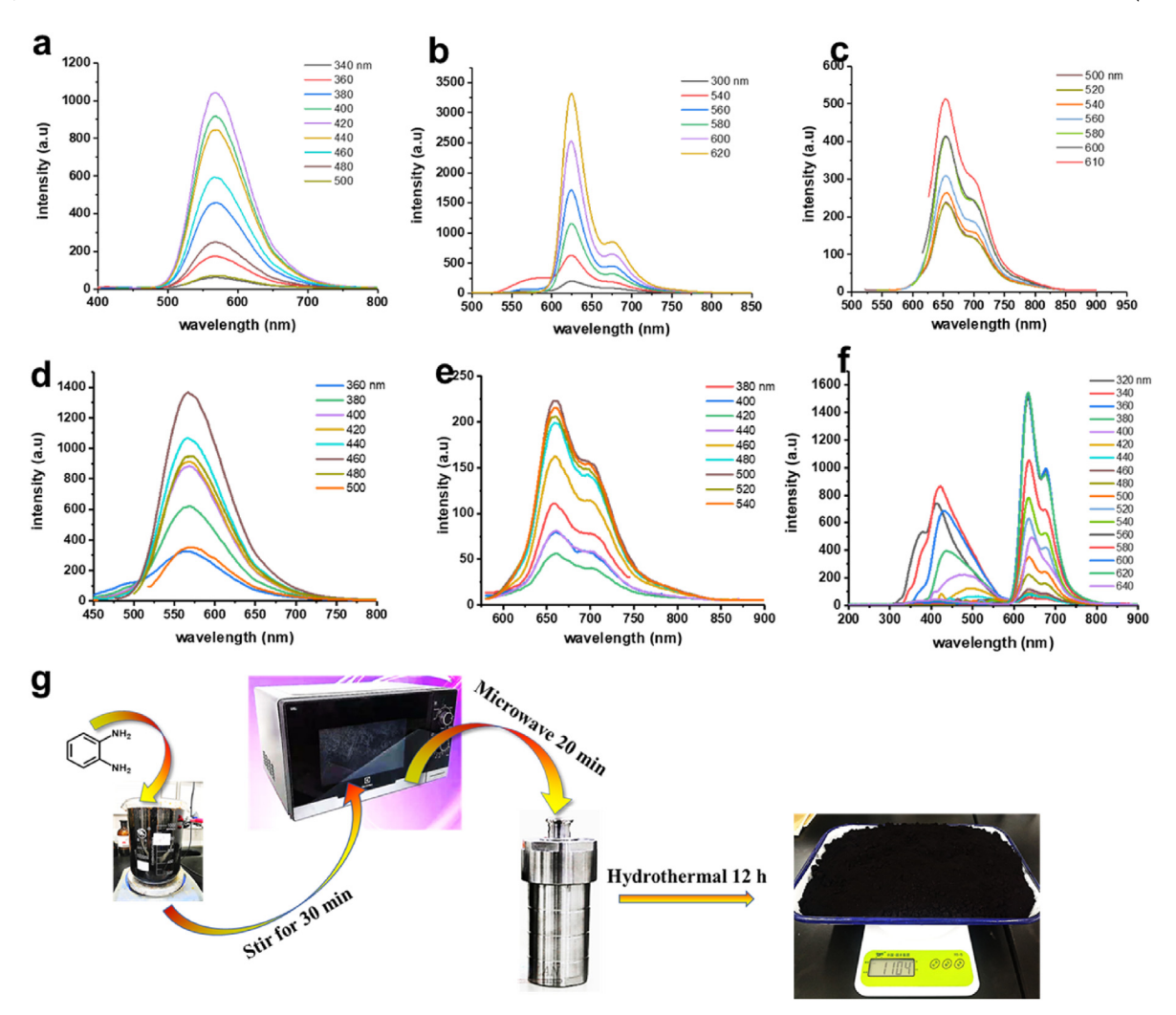


Fig. 1. a) Fluorescence (FL) emission spectra of C-dots₅₆₈. **b**) FL spectra of C-dots₆₂₆. **c**) FL spectra of C-dots₆₅₃ obtained by microwave irradiation followed by hydrothermal treatment. **d**) FL spectra of C-dots obtained from *o*-PDA *via* microwave irradiation followed by hydrothermal treatment in a non-acidic environment. **e**) FL spectra of C-dots₆₅₃ obtained by microwave irradiation followed by hydrothermal treatment in a non-oxidizing environment. **f**) FL spectra of C-dots₆₅₃ synthesized without microwave pretreatment **g**) schematic illustration showing the synthesis process of C-dots₆₀₆ on a kilogram-scale. (A colour version of this figure can be viewed online.)

turned to deep red when excited by a 365 nm handheld UV lamp (Fig. 2c, insets). The fluorescence spectra show that C-dots₆₀₆

demonstrate fluorescence emissions independent of the excitation wavelengths. Specifically, no matter how the excitation

Table 1Table showing the different parameters for C-dots syntheses and the corresponding emission wavelengths and yields of C-dots formed.

	C-dots b)	Acid	Oxidant ^{c)}	Microwave irradiation d)	Hydrothermal treatment	Emission (nm)	Yield (%)
1	C-dots ₅₆₈	-	-	MS	no	568	_
2	C-dots ₆₂₆	HCl	TBHP	MS	no	626	_
3	C-dots ₆₅₃	HCl	TBHP	MS	yes	653	86
4	C-dots ₆₅₃	_	TBHP	MS	yes	_	0
5	C-dots ₆₅₃	HCl	_	MS	yes	653	23
6	C-dots ₆₅₃	HCl	TBHP	_	yes	653	46
7	C-dots ₆₅₃	HCl	TBHP	DM	yes	653	34
8 a)	C-dots ₆₅₃	H_2SO_4	m-CPBA	DM	yes	653	65
9 a)	C-dots ₆₀₆	H_2SO_4	m-CPBA	DM	yes	606	94
10	C-dots ₆₀₆	H_2SO_4	m-CPBA	DM	yes	606	96

a) The two reactions were carried out under identical conditions while their post-processing was slightly different. For reaction in **row 8**, the resulted reaction mixture was directly filtered and the residues were washed, collected and vacuum dried to result C-dots₆₅₃ as black powders in relatively lower yield; while for reaction in **row 9**, the pH of the resulted reaction mixture was first adjusted to neutral, then the mixture was filtered and the residues were washed, collected and vacuum dried to result C-dots₆₀₆ as black powders in quantitative yield

powders in quantitative yield.

b) Reactions in **rows 1–9** were carried out in small scale, which only used 0.25 g of *o*-PDA for each reaction; while reaction in **row 10** was carried out on a kilogram-scale, which used 1.15 Kg of *o*-PDA and produced 1.1 Kg of C-dots₆₀₆.

c) TBHP: *tert*-butyl hydroperoxide; *m*-CPBA: 3-chloroperbenzoic acid.

d) MS: microwave synthesizer; DM: domestic microwave.

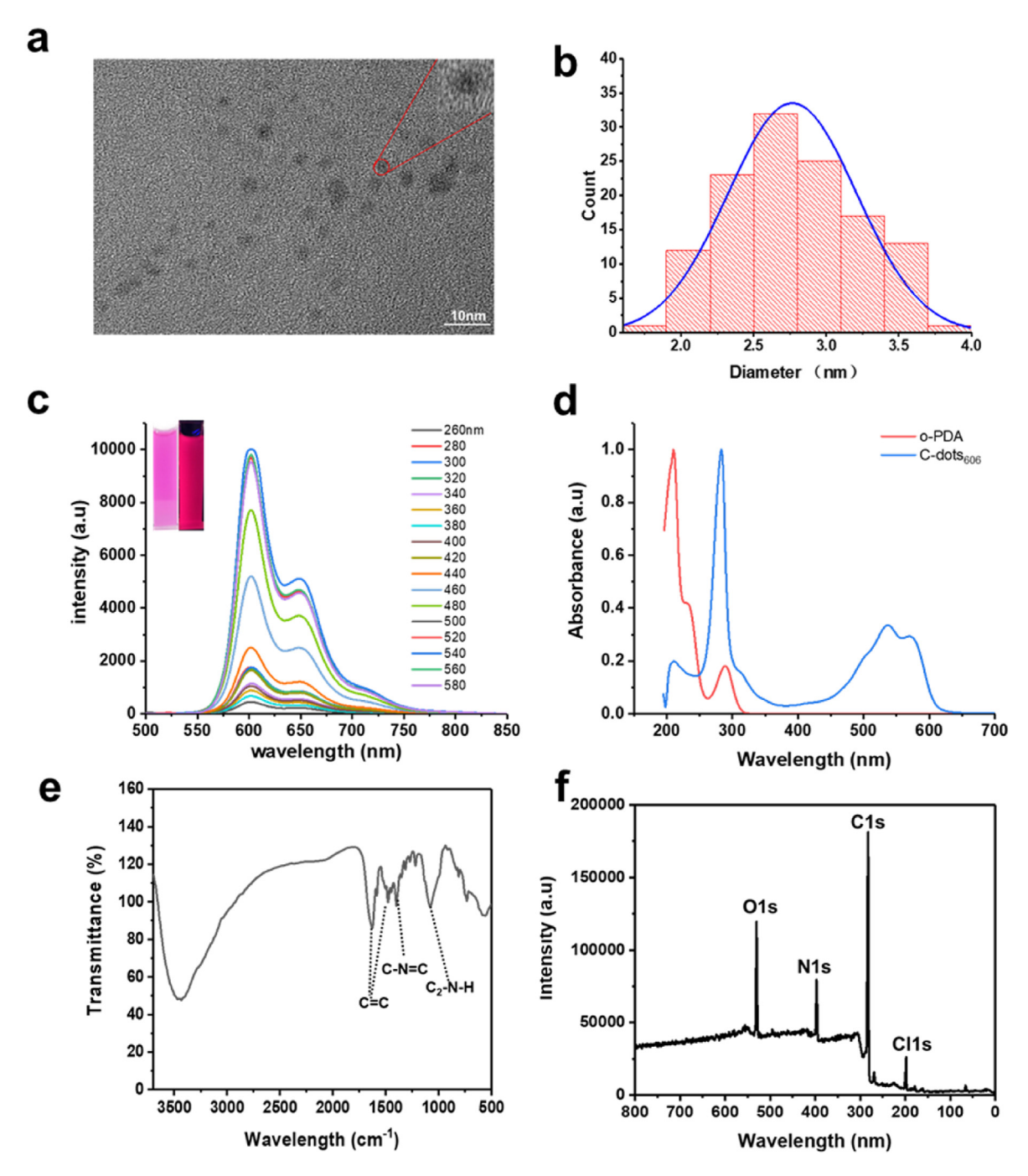


Fig. 2. a) TEM image of C-dots₆₀₆, the inset is an enlarged view of a particle. **b**) The size distribution histogram of C-dots₆₀₆. **c**) PL spectra of C-dots₆₀₆ excited at various wavelengths, the insets: photograph of C-dots₆₀₆ under ambient light (left) and 365 nm handheld UV light (right). **d**) UV—vis spectra of C-dots₆₀₆ and o-PDA. **e**) The FTIR spectra of C-dots₆₀₆. **f**) XPS survey spectra of C-dots₆₀₆. (A colour version of this figure can be viewed online.)

wavelengths move, the emissions always present the main peaks at 606 nm and shoulder peaks at 653 nm (Fig. 2c). The fluorescence lifetime and QY of the sample were determined to be 1.38 ns, and 25.4%, respectively. The UV—vis absorption spectrum shows that C-dots₆₀₆ have two absorption peaks at 235 and 280 nm in the UV region, which could be attributed to the n- π * transition of C—NH₂ and the π - π * transition of C—C/C—N, respectively. The absorption peaks higher than 400 nm were attributed to the complex surface states of C-dots₆₀₆ (Fig. 2d) [8,41]. Compared with the precursor o-PDA, the peak of C-dots₆₀₆ at 235 nm decreased significantly while that at 280 nm increased greatly. This phenomenon could be

attributed to the consumption of C $-NH_2$ (absorption at 235 nm) and the simultaneous formation of C-C/C=N (absorption at 280 nm) due to the polymerization and carbonization in the process of C-dots formation. To our delight, FTIR and XPS spectra also confirmed the formation of the above-discussed structures.

In the FTIR spectrum (Fig. 2e), the absorption peak at 3440 cm⁻¹ was assigned to the N–H vibration of the amino functional groups. The absorption peaks at 1630 and 1477 cm⁻¹ could be attributed to the C=C bonds of the conjugated system [20]. There is an obvious absorption peak at 1394 cm⁻¹, which could be attributed to the C–N=C that is typical for the phenazine structure. The absorption

peak at 1074 cm⁻¹ could be attributed to the secondary amine functional group. Based on the FTIR spectra, we could reasonably conclude that a large number of phenazine structures and some unreacted amino functional groups are presented on the surface of the C-dots. XPS spectroscopy further confirms these functionalities. The full scan XPS spectrum (Fig. 2f) shows that the C-dots are mainly composed of C (73.65%), N (11.71) and O (11.86%). Furthermore, the high-resolution C1s XPS spectrum (Fig. S3) shows the presence of four different types of C: C-C/C=C (284.70 eV), C-O/ C-N (285.73 eV), C=N/C=0 (286.86 eV) [21], which also supports the presence of phenazine and amino moieties on C-dots₆₀₆ as FTIR spectrum indicated. The high-resolution N1s spectrum (Fig. S4) shows three peaks at 399.29 eV, 400.31 eV and 401.03eV which are corresponding to pyridine, pyrrole and graphitic nitrogens, respectively [20]. The high-resolution O1s spectrum (Fig. S5) shows two different types of O: C-O (531.92 eV), C=O (532.75 eV), which indicates that the surfaces of C-dots₆₀₆ contain some amount of hydroxyl and carboxyl groups.

3.3. C-dots formation process and structural model

It has been reported in several studies that two molecules of o-PDA could self condense to form the dimer 2, 3-diaminophenazine (DAP, substance 2 in Fig. 3) under acidic conditions [42–45]. This was probably what initially happened in our synthesis during the stirring of the reaction mixtures before microwave irradiation and hydrothermal treatment. Indeed, our control experiment in which o-PDA was stirred in an acidic solution did produce DAP that emitted at 568 nm (Fig. S6). Under desired conditions, the DAP could further condense to form even larger molecules (i.e., dimers of DAP). According to previous study, the horizontal and vertical polymerization forming C-N bonds are thermodynamically more favorable than other polymerization types (i.e., forming N-N bonds) [46]. In our study, the C-dots synthesized after microwave irradiation (C-dots₆₂₆) were believed to be such dimers of DAP. Cdots₆₂₆ were quite unstable and quickly deteriorated, as a result, we failed to obtain solid samples and carry out full characterizations of C-dots₆₂₆. Luckily, we successfully obtained single crystals from the solution of C-dots₆₂₆ which was determined to be DAP via single crystal XRD diffraction (Fig. S7, Table S3). In addition, the solution of the crystals also demonstrated same fluorescence emission of that of DAP (Fig. S8). These observations supported our assignment of Cdots₆₂₆ as the dimers of DAP (substance 3 or 4, Fig. 3), which was not stable and would decompose back to DAP (C-dots₅₆₈). Furthermore, in the matrix-assisted laser desorption ionization time-of-light mass spectrometry (MALDI-TOFMS) analysis of C-

dots₆₀₆, we observed major peaks located at m/z = 415.143 and 416.136 (Fig. S9), which could be attributed to the protonated dimers of DAP (substance **3** or **4**, Fig. 3).

Based on the above discussions, the possible formation process of C-dots₆₀₆ was proposed: under acidic conditions, two molecules of o-PDA could self condense to form DAP (C-dots₅₆₈, substance 2 in Fig. 3) under acidic conditions. With the assistance of oxidization agents (i.e., m-CPBA) and microwave irradiation, o-PDA and DAP were further polymerized to form heavier fragments (C-dots₆₂₆, substance 3 or 4, Fig. 3), which were thermodynamically not stable enough and subjected to easy deterioration. In situ hydrothermal treatment of these fragments (C-dots₆₂₆) could provide an environment for them to further polymerize and cross link with each other to form C-dots₆₅₃, which significantly enhanced their stabilities [47]. During this process, there might be partial carbonization of the carbon core. Basic work-up of C-dots₆₅₃ would result the final products C-dots₆₀₆ (Fig. 3). Indeed, in the X-ray diffraction pattern (XRD), C-dots₆₀₆ not only show a typical broad peak at around 25°, which is indicative of amorphous carbon; but also present many sharp narrow peaks, which are more like diffraction patterns of ordered, polymeric structures (Fig. S10). Thus, XRD shows that Cdots₆₀₆ not only contain a certain degree of carbon core structure but also have a large number of surface polymeric structures. Furthermore, both the characteristic D (1355 cm-1) and G (1590 cm-1) bands and other bands representing polymeric materials are present in the Raman spectrum of C-dots₆₀₆, indicating that they were not typical graphitic derivatives (Fig. S11). Collectively speaking, the C-dots could be regarded as the clusters of dimers of DAP piled up in an orderly manner to form layered graphite-like structures without excessive carbonization, which still retained significant amount of the characteristic phenazine structures.

3.4. Facile tuning of optical properties and the mechanism

To our delight, the as-prepared C-dots (C-dots₆₀₆) were very sensitive to pH and this phenomenon could be exploited to facilely tune the optical properties of C-dots₆₀₆. As demonstrated (Fig. 4a), C-dots₆₀₆ solution was pink under a fluorescent lamp, and it turned to blue once the solution was acidified. Upon acidified, both the UV—vis absorption and fluorescence emission spectra of C-dots₆₀₆ were red shifted. Specifically, a strong new absorption peak at 628 nm was observed in the absorption spectrum (Fig. 4b, black line), and the best fluorescence emission peak was red-shifted from 606 to 653 nm (Fig. 4c). NIR C-dots are highly desired for bioimaging and optoelectronic devices fabrication, thus the ability to red shift the emission of C-dots₆₀₆ by a great extent (47 nm) via

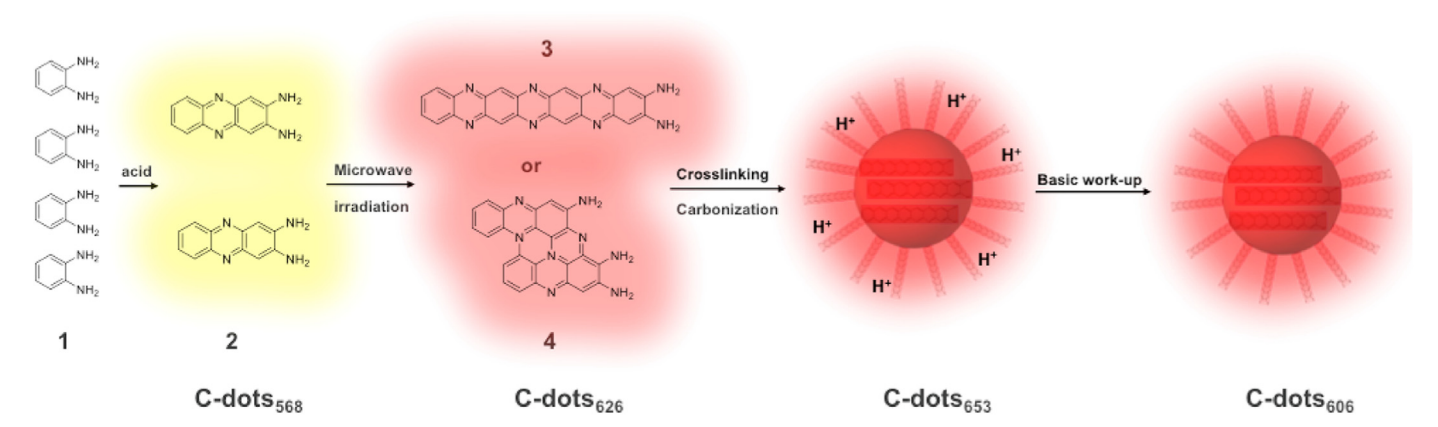


Fig. 3. Schematic diagram showing the proposed C-dots₆₀₆ formation processes.

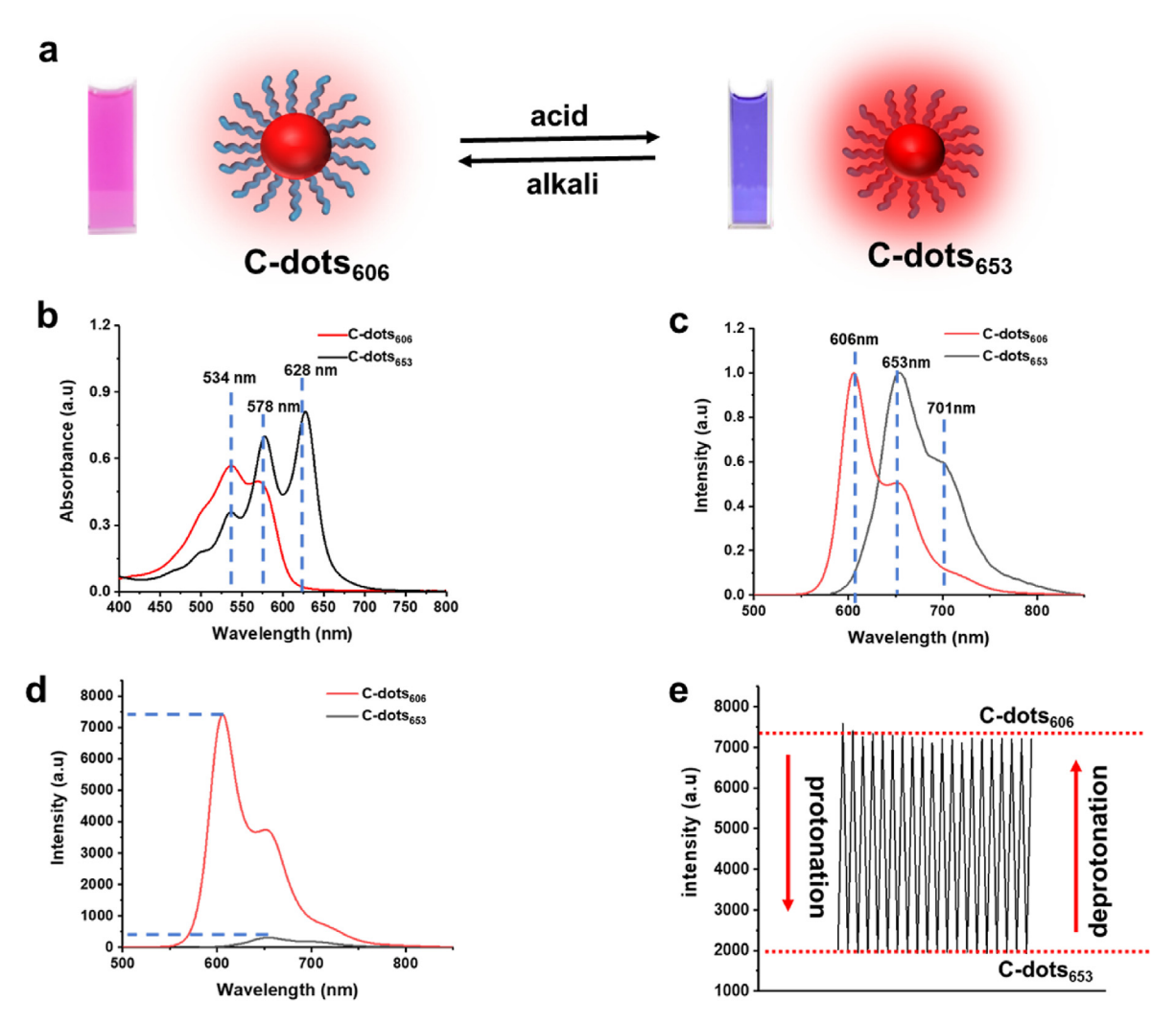


Fig. 4. a) Schematic diagram showing the transformation between C-dots₆₀₆ and C-dots₆₅₃ under different conditions. **b)** UV—vis spectra of C-dots₆₀₆ (red) and C-dots₆₅₃ (black). **c)** Normalized PL spectra of C-dots₆₀₆ (red) and C-dots₆₅₃ (black). **d)** PL spectra of C-dots₆₀₆ (red) and C-dots₆₅₃ (black) which were not normalized. **e)** PL intensities of C-dots₆₀₆ (top) and C-dots₆₅₃ (bottom) during 20 cycles of transformation. (A colour version of this figure can be viewed online.)

simple acidification is truly exciting. On the other hand, when the acidified C-dots (C-dots₆₅₃) were treated with base and deacidified, their emission was quickly blue shifted back to 606 nm, with the fluorescence intensity increased by 11 times (Fig. 4d), and the QY increased from 8.1 to 25.4%. To our delight, there was almost no change in their fluorescence intensities after 20 cycles of acidification, de-acidification (Fig. 4e), demonstrating the high reversibility and applicability of this optical tuning approach.

To elucidate the nature of the facile tuning of the optical properties, FTIR and Zeta potential tests were performed on the acidified C-dots (C-dots₆₅₃). In the FTIR spectra, C-dots₆₅₃ showed two new absorption peaks at 605 and 745 cm⁻¹, which could be assigned to the N–H stretching vibrations of the phenazine structure (Fig. 5a) [20]. The Zeta potential of C-dots₆₅₃ was +30.1 mV while that of C-dots₆₀₆ was -12.5 mV indicating C-dots₆₅₃ was indeed heavily protonated. The DLS hydrodynamic diameters of C-dots₆₀₆ and C-dots₆₅₃ were determined to be 3.38 and 3.15 nm, respectively (Figs. S12 and S13), which could rule out the possibility that the aggregation of C-dots₆₀₆ lead to the red shift and lower QY. Furthermore, our study showed that simple treatment of C-dots₆₅₃ with non-nucleophilic bases such as N, N-Diisopropylethylamine (DIPEA) or 1,8-Diazabicyclo [5.4.0] undec-7-ene (DBU) could easily

restore the optical features of C-dots₆₀₆ (Fig. S14). Collectively consider these characterizations and the fact the tuning of the optical properties were nondestructive and highly reversible (Fig. 4e), a reasonable process was proposed for this tuning: there were large quantities of amino and phenazine moieties on the surface of C-dots₆₀₆, and the phenazine structures could pick up protons to form N–H structure, which could alter the surface states of C-dots₆₀₆. In summary, the optical properties tuning of our C-dots could be reasonably regarded as a protonation-deprotonation process.

Indeed, the UV—vis absorption and fluorescence spectra of the protonated C-dots (C-dots₆₅₃) in different solvents also supported the conclusion that the optical tuning was a protonation-deprotonation process. Specifically, we found that the UV—vis absorption spectra of C-dots₆₅₃ in methanol/ethanol had an obvious red shift compared to the dispersions in DMF and DMSO (Fig. 5b). This could be well explained in a protonation-deprotonation process, since DMF and DMSO are aprotic solvents with good deprotonation capabilities, which could cause the deprotonation of C-dots₆₅₃, thus causing the shift of the UV—vis absorption. As expected, we observed the fluorescence emissions of C-dots₆₅₃ in protic solvents (methanol and ethanol) were red shifted greatly

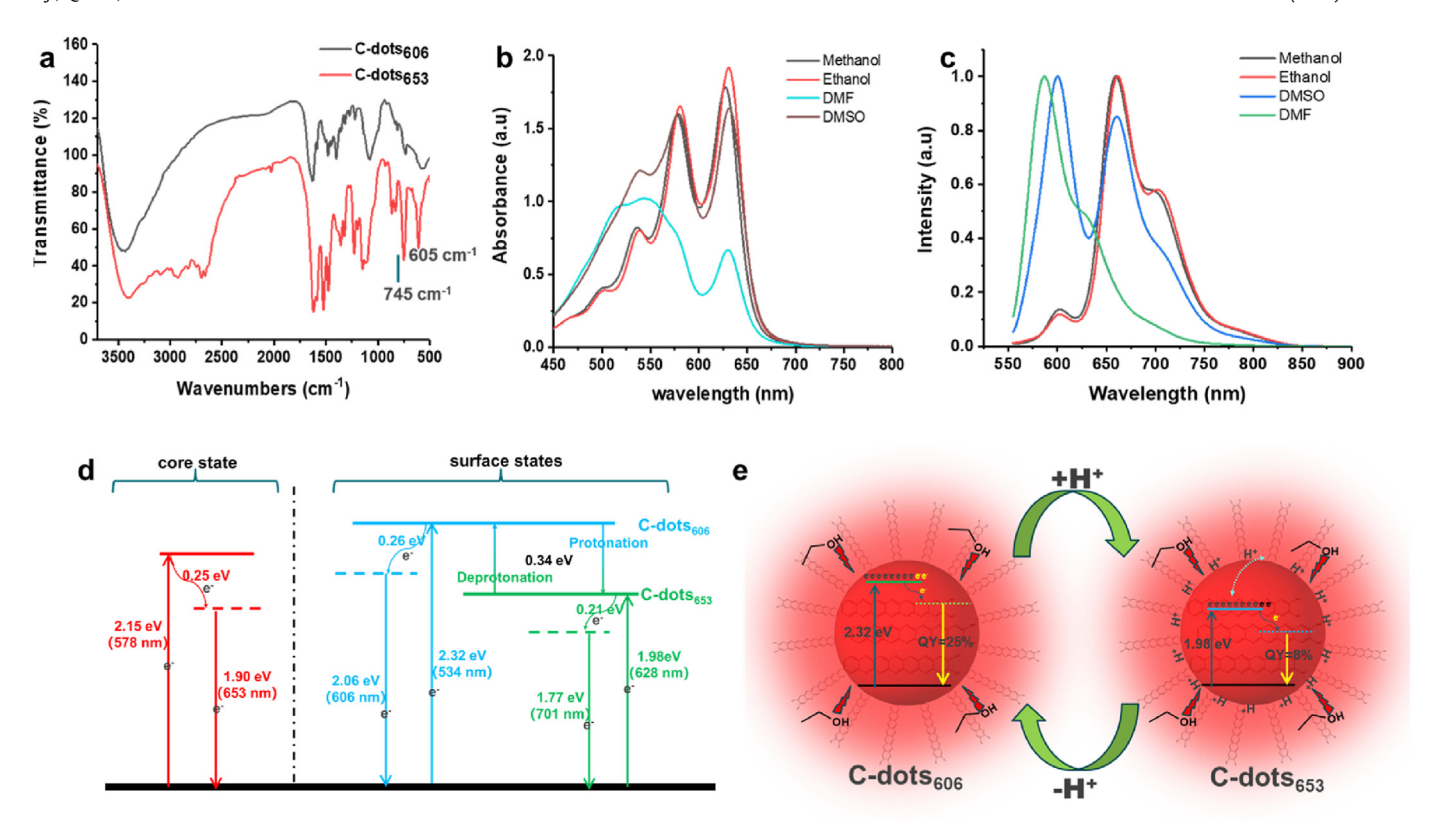


Fig. 5. a) FTIR spectra of C-dots₆₀₆ and C-dots₆₅₃, **b)** UV–vis spectra of C-dots₆₅₃ in different solvents, **c)** Normalized PL spectra of C-dots₆₅₃ in different solvents, **d)** Schematic diagram showing the proposed electronic transition states of C-dots₆₀₆ and C-dots₆₅₃, **e)** Schematic diagram showing the proposed mechanism in which protonation and deprotonation influenced the fluorescence emissions of C-dots₆₀₆ and C-dots₆₅₃. (A colour version of this figure can be viewed online.)

relative to that in aprotic solvents DMF and DMSO (Fig. 5c).

A close look at the UV-vis absorption and fluorescence emission spectra of the sample during the protonation-deprotonation process revealed something very interesting. Specifically, the UV-vis absorption peak at 578 nm of C-dots₆₀₆ did not move at all after protonation, while the absorption peak at 534 nm was red-shifted to 628 nm (Fig. 4b). Similarly, the shoulder fluorescence emission peak at 653 nm of C-dots₆₀₆ stayed the same while the main emission peak at 606 nm was red-shifted to 701 nm after protonation (Fig. 4c). Based on these observations, we speculate that the C-dots in our study might have two major fluorescent emission centers: one is the core state, the bandgap of which is hardly affected by surface protons, and the other is the surface state, which is easily influenced by surface protonation. As such, the emission at 653 nm was attributed to the core state luminescence, while the peaks at 606 and 701 nm were attributed to the surface state emissions of C-dots₆₀₆ (deprotonated state) and C-dots₆₅₃ (protonated state), respectively.

Next, we calculated the band gaps of these emissions and a diagram showing the electronic transition states of the C-dots was proposed (Fig. 5d). Specifically, the band gaps corresponding to the emissions of the C-dots were calculated following the formula $E_g^{opt}=1340/\lambda_{edge}$ [44]. In the core state emissions (Fig. 5d, transitions in red), electrons in the ground state were promoted to the excited state after absorbing 2.15 eV of energy, which later on released 0.25 eV of non-radiative energy and eventually went back to ground state by losing 1.90 eV of energy in the form of light emissions. The process is not affected by the surface protonation and deprotonation, thus behaved quite similarly in both C-dots₆₀₆ and C-dots₆₅₃. On the other hand, the surface state emissions were heavily influenced by the surface protonation and deprotonation

(Fig. 5d, transitions in blue and green). Specifically, electrons of C-dots₆₀₆ in the ground state could be promoted to the excited state by absorbing 2.32 eV of energy, among which 0.26 eV was lost *via* non-radiative decay and 2.06 eV was released as emission lights when the electrons returned to ground state (Fig. 5d, transitions in blue). After protonation, the excited state was lowered; as a result, only 1.98 eV of energy could promote the ground electrons to the excited state. The excited electrons could lose 0.21 eV during non-radiative decay and 1.77 eV was released as emission lights (Fig. 5d, transitions in green). Accordingly to the calculations, there was 0.34 eV of energy difference in the excited states of the C-dots₆₀₆ and C-dots₆₅₃.

We further measured the fluorescence lifetime of the samples (Fig. S15), and the result showed that C-dots₆₀₆ (at 606 nm) and Cdots₆₅₃ (at 701 nm) had fluorescence lifetime of 1.38 and 2.38 ns, respectively. Furthermore, the PLOYs of C-dots₆₀₆ and C-dots₆₅₃ under identical conditions were measured to be 25.4 and 8.1%, respectively. As is known, the fluorescence lifetime of a fluorophore is largely depending on the time the promoted electrons spent on the excited state, while the PLQY relies on the ratio of excited electrons that return to the ground state via radiative pathways. Collectively consider the data we obtained and the above discussions, a reasonable model (Fig. 5e) was proposed to explain the differences between the native (C-dots₆₀₆) and protonated C-dots (C-dots₆₅₃). In C-dots₆₅₃, the excited state was relatively stable because the presence of surface protons could stabilize the highenergy excited electrons; while that of C-dots₆₀₆ was less stable because there were no surface protons to stabilize the excited electrons except the solvation effect. As a result, the excited state of C-dots₆₀₆ was higher in energy than that of C-dots₆₅₃, which was in accordance with our calculations above. Also, with the stabilization

effect from the surface protons, the electrons could spend more time in the excited state, resulting in a longer fluorescence lifetime for C-dots₆₅₃. However, with the strong interaction with the surface protons, large quantities of excited electrons could return to the ground state *via* non-radiative pathways, and thus the PLQY of C-dots₆₅₃ was significantly lower than that of C-dots₆₀₆. Similar results have been reported in literature in which surface protonation/pH have appeared to influence the PL properties of C-dots, and depending on the nature of the PL (i.e., core state, surface state), the influences of protonation/pH were quite different [48–51]. For instance, Jin et al. investigated the pH influence on the fluorescence lifetime and QY of C-dots, and it was revealed that high pH would lead to a decrease in the fluorescence lifetime and an increase in the QY of C-dots [48].

3.5. C-dots as phosphors for red LED construction

Considering the excellent red-emissive capability, kilogramscale and low cost synthesis, C-dots₆₀₆ were used as cheap and readily available red phosphors to construct red LEDs to demonstrate their application (Fig. 6). To avoid their fluorescence quenching in the solid state, polyvinylpyrrolidone (PVP) was used as a dispersant for C-dots₆₀₆ to prepare phosphors, which were reddish brown under ambient light and emitted bright red light under a 365 nm handheld ultraviolet lamp (Fig. 6a, b). The obtained phosphors were then used to assemble red LED with a blue LED chip (382 nm). To our delight, the red LED was very effective and emitted warm red light (Fig. 6c). The luminescence spectrum showed that the light emitted by the LED was mainly in the red range (Fig. 6d), and the red light component accounted for more than 70% of the total emissions (Fig. 6e). Furthermore, the CIE coordinates (0.58, 0.42) of the light (Fig. 6f) was very close to the coordinates of the standard red luminescence, demonstrating the high potential of C-dots₆₀₆ as cheap and readily available red phosphors for the construction of red and while LEDs.

4. Conclusions

In this study, low-cost (\$0.1 for each gram) preparation of NIR Cdots from o-PDA at kilogram-scale with high yield was achieved via a combinative microwave-hydrothermal treatment. The desired Cdots that emitted red light could be facilely isolated and purified *via* pH adjusting and filtering. Careful study showed that two molecules of o-PDA could self condense to form DAP (emitting at 568 nm) in acidic condition, and the DAP molecules could further polymerize to form dimers (emitting at 626 nm) upon microwave irradiation. These dimers were thermodynamically unstable and they could further polymerize and cross link with each other to form the stable C-dots after in situ hydrothermal treatment. To our delight, the optical properties of the C-dots could also be facilely tuned via simple protonation-deprotonation manipulation. The protonation of the as-prepared C-dots (C-dots₆₀₆) could readily red shift the emissions by 47 nm and greatly increase the fluorescence lifetime, which could be attributed to the stabilization of the excited electrons by the surface protons. According to the calculated band gaps of the emissions, diagrams showing the electronic transition states of the as prepared (C-dots₆₀₆) and protonated (Cdots₆₅₃) C-dots were proposed. The as prepared C-dots were used as cheap and readily available phosphors for the assembling of red LEDs. The red light component of the LED accounted for more than 70% of the total emissions and the CIE coordinates of the LED light was very close to the coordinates of the standard red luminescence. In short, a kilogram-scale synthesis of NIR C-dots, their facile optical properties tuning and application as phosphors for red LED construction was reported, in which the formation process and structural model of C-dots as well as the mechanism for optical properties tuning were proposed.

CRediT authorship contribution statement

Chunyu Ji: Investigation, Methodology, Formal analysis, Writing

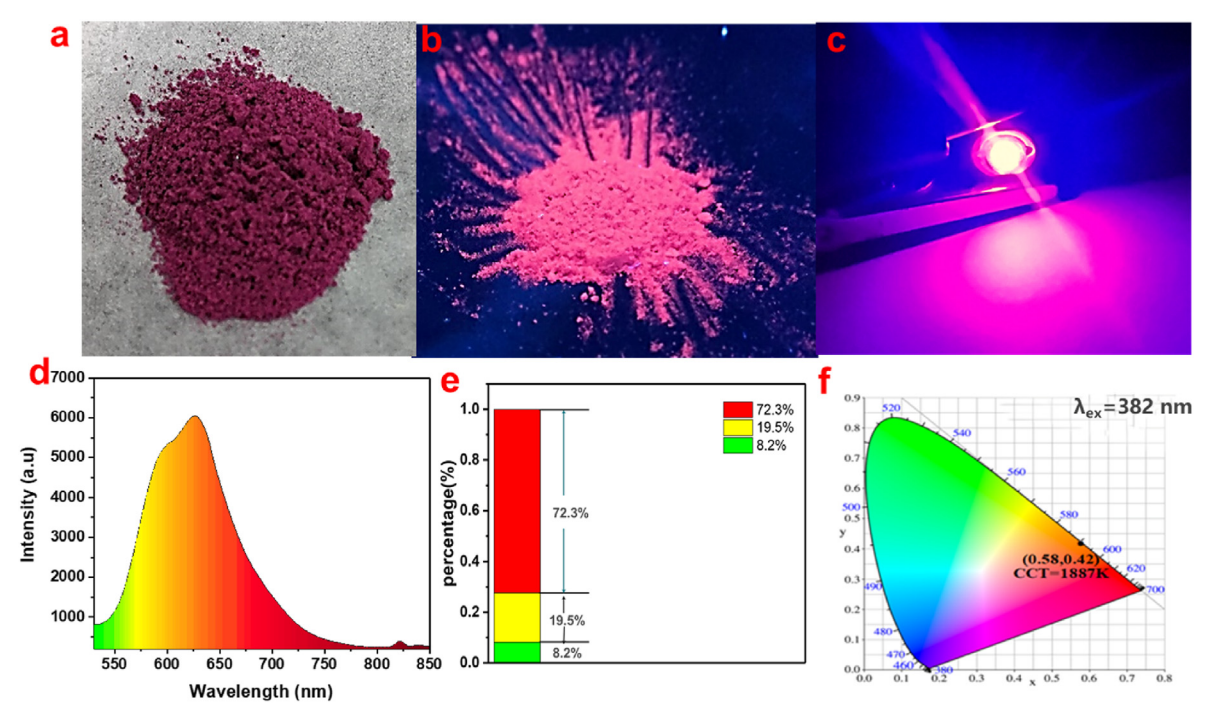


Fig. 6. a) Phosphors prepared from C-dots₆₀₆ showing reddish brown color in daylight. **b**) Phosphors prepared from C-dots₆₀₆ emitting red light when excited by a 365 nm handheld UV lamp. **c**) Red LEDs constructed with a blue LED chip (382 nm) and C-dots₆₀₆-derived phosphors. **d**) The fluorescence spectrum of the light emitted by the red LED. **e**) The proportion of each color in the light emitted by the red LED. **f**) The color coordinate (CIE) of the light emitted by the red LED. (A colour version of this figure can be viewed online.)

original draft. Qiurui Han: Investigation, Methodology, Formal analysis, Writing – review & editing. Yiqun Zhou: Investigation, Methodology, Formal analysis. Jiajia Wu: Investigation, Formal analysis. Wenquan Shi: Investigation, Formal analysis. Lipeng Gao: Formal analysis, Formal analysis, Roger M. Leblanc: Supervision, Project administration, Funding acquisition. Zhili Peng: Conceptualization, Formal analysis, Writing – review & editing, Supervision, Project administration. Funding acquisition.

Declaration of competing interest

The authors declare that they have no known competing financial interests or personal relationships that could have appeared to influence the work reported in this paper.

Acknowledgements

Z. Peng gratefully acknowledge the financial support from the National Natural Science Foundation of China under the grant number: 21807010, and the Applied Basic Research Program of Yunnan Province under the grant number: 2019FB066. R. M. Leblanc gratefully acknowledges the support of the National Science Foundation under Grants 1809060 and 2041413. Authors thank Advanced Analysis and Measurement Center of Yunnan University for the sample testing service.

Appendix A. Supplementary data

Supplementary data to this article can be found online at https://doi.org/10.1016/j.carbon.2022.02.054.

References

- [1] X. Xu, R. Ray, Y. Gu, H.J. Ploehn, L. Gearheart, K. Raker, W.A. Scrivens, Electrophoretic analysis and purification of fluorescent single-walled carbon nanotube fragments, J. Am. Chem. Soc. 126 (40) (2004) 12736–12737.
- [2] Y.-P. Sun, B. Zhou, Y. Lin, W. Wang, K.S. Fernando, P. Pathak, M.J. Meziani, B.A. Harruff, X. Wang, H. Wang, Quantum-sized carbon dots for bright and colorful photoluminescence, J. Am. Chem. Soc. 128 (24) (2006) 7756–7757.
- [3] L. Yue, H. Li, Q. Sun, J. Zhang, X. Luo, F. Wu, X. Zhu, Red-emissive ruthenium-containing carbon dots for bioimaging and photodynamic cancer therapy, ACS Appl. Nano Mater. 3 (1) (2020) 869–876.
- [4] S.D. Hettiarachchi, R.M. Graham, K.J. Mintz, Y. Zhou, S. Vanni, Z. Peng, R.M. Leblanc, Triple conjugated carbon dots as a nano-drug delivery model for glioblastoma brain tumors, Nanoscale 11 (13) (2019) 6192–6205.
- [5] C. Ji, Y. Zhou, R.M. Leblanc, Z. Peng, Recent developments of carbon dots in biosensing: a review, ACS Sens. 5 (9) (2020) 2724–2741.
- [6] M. Vazquez-Gonzalez, W.C. Liao, R. Cazelles, S. Wang, X. Yu, V. Gutkin, I. Willner, Mimicking horseradish peroxidase functions using Cu(2+)-modified carbon nitride nanoparticles or Cu(2+)-modified carbon dots as heterogeneous catalysts, ACS Nano 11 (3) (2017) 3247–3253.
- [7] J. Guo, H. Li, L. Ling, G. Li, R. Cheng, X. Lu, A.-Q. Xie, Q. Li, C.-F. Wang, S. Chen, Green synthesis of carbon dots toward anti-counterfeiting, ACS Sustain. Chem. Eng. 8 (3) (2019) 1566–1572.
 [8] B. Wang, J. Yu, L. Sui, S. Zhu, Z. Tang, B. Yang, S. Lu, Rational design of multi-
- [8] B. Wang, J. Yu, L. Sui, S. Zhu, Z. Tang, B. Yang, S. Lu, Rational design of multicolor-emissive carbon dots in a single reaction system by hydrothermal, Adv. Sci. 8 (1) (2021) 2001453.
- [9] X. Li, H. Wang, Y. Shimizu, A. Pyatenko, K. Kawaguchi, N. Koshizaki, Preparation of carbon quantum dots with tunable photoluminescence by rapid laser passivation in ordinary organic solvents, Chem. Commun. 47 (3) (2010) 932–934.
- [10] H. Gonçalves, J.C.E. da Silva, Fluorescent carbon dots capped with PEG 200 and mercaptosuccinic acid, J. Fluoresc. 20 (5) (2010) 1023–1028.
- [11] Z.-A. Qiao, Y. Wang, Y. Gao, H. Li, T. Dai, Y. Liu, Q. Huo, Commercially activated carbon as the source for producing multicolor photoluminescent carbon dots by chemical oxidation, Chem. Commun. 46 (46) (2010) 8812–8814.
 [12] X.-J. Mao, H.-Z. Zheng, Y.-J. Long, J. Du, J.-Y. Hao, L.-L. Wang, D.-B. Zhou, Study
- [12] X.-J. Mao, H.-Z. Zheng, Y.-J. Long, J. Du, J.-Y. Hao, L.-L. Wang, D.-B. Zhou, Study on the fluorescence characteristics of carbon dots, Spectrochim. Acta, Part A 75 (2) (2010) 553–557.
- [13] H. Li, X. He, Z. Kang, H. Huang, Y. Liu, J. Liu, S. Lian, C.H.A. Tsang, X. Yang, S.T. Lee, Water-soluble fluorescent carbon quantum dots and photocatalyst design, Angew. Chem. Int. Ed. 49 (26) (2010) 4430–4434.
- [14] J. Xia, S. Chen, G.-Y. Zou, Y.-L. Yu, J.-H. Wang, Synthesis of highly stable redemissive carbon polymer dots by modulated polymerization: from the mechanism to application in intracellular pH imaging, Nanoscale 10 (47)

(2018) 22484-22492.

- [15] L. Pan, S. Sun, A. Zhang, K. Jiang, L. Zhang, C. Dong, Q. Huang, A. Wu, H. Lin, Truly fluorescent excitation-dependent carbon dots and their applications in multicolor cellular imaging and multidimensional sensing, Adv. Mater. 27 (47) (2015) 7782–7787.
- [16] Y. Song, S. Zhu, S. Zhang, Y. Fu, L. Wang, X. Zhao, B. Yang, Investigation from chemical structure to photoluminescent mechanism: a type of carbon dots from the pyrolysis of citric acid and an amine, J. Mater. Chem. C 3 (23) (2015) 5976—5984
- [17] J. Schneider, C.J. Reckmeier, Y. Xiong, M. von Seckendorff, A.S. Susha, P. Kasák, A.L. Rogach, Molecular fluorescence in citric acid-based carbon dots, J. Phys. Chem. C 121 (3) (2017) 2014–2022.
- [18] H. Wang, M. Zhang, Y. Ma, B. Wang, H. Huang, Y. Liu, M. Shao, Z. Kang, Carbon dots derived from citric acid and glutathione as a highly efficient intracellular reactive oxygen species scavenger for alleviating the lipopolysaccharideinduced inflammation in macrophages, ACS Appl. Mater. Interfaces 12 (37) (2020) 41088–41095.
- [19] K. Jiang, S. Sun, L. Zhang, Y. Lu, A. Wu, C. Cai, H. Lin, Red, green, and blue luminescence by carbon dots: full-color emission tuning and multicolor cellular imaging, Angew. Chem., Int. Ed. Engl. 54 (18) (2015) 5360-5363.
- [20] J. Liu, D. Li, K. Zhang, M. Yang, H. Sun, B. Yang, One-step hydrothermal synthesis of nitrogen-doped conjugated carbonized polymer dots with 31% efficient red emission for in vivo imaging, Small 14 (15) (2018) 1703919.
- [21] H. Jia, Z. Wang, T. Yuan, F. Yuan, X. Li, Y. Li, Z.a. Tan, L. Fan, S. Yang, Electroluminescent warm white light-emitting diodes based on passivation enabled bright red bandgap emission carbon quantum dots, Adv. Sci. 6 (13) (2019) 1900397.
- [22] F. Yuan, T. Yuan, L. Sui, Z. Wang, Z. Xi, Y. Li, X. Li, L. Fan, Z.a. Tan, A. Chen, Engineering triangular carbon quantum dots with unprecedented narrow bandwidth emission for multicolored LEDs, Nat. Commun. 9 (1) (2018) 1–11.
- [23] F. Yuan, P. He, Z. Xi, X. Li, Y. Li, H. Zhong, L. Fan, S. Yang, Highly efficient and stable white LEDs based on pure red narrow bandwidth emission triangular carbon quantum dots for wide-color gamut backlight displays, Nano Res. 12 (7) (2019) 1669–1674.
- [24] Z. Wang, F. Yuan, X. Li, Y. Li, H. Zhong, L. Fan, S. Yang, 53% efficient red emissive carbon quantum dots for high color rendering and stable warm white-light-emitting diodes, Adv. Mater. 29 (37) (2017) 1702910.
- [25] J. Ge, Q. Jia, W. Liu, L. Guo, Q. Liu, M. Lan, H. Zhang, X. Meng, P. Wang, Redemissive carbon dots for fluorescent, photoacoustic, and thermal theranostics in living mice, Adv. Mater. 27 (28) (2015) 4169–4177.
- [26] S. Zhao, K. Yang, L. Jiang, J. Xiao, B. Wang, L. Zeng, X. Song, M. Lan, Polythiophene-based carbon dots for imaging-guided photodynamic therapy, ACS Appl. Nano Mater. 4 (10) (2021) 10528–10533.
- [27] J. Ge, Q. Jia, W. Liu, M. Lan, B. Zhou, L. Guo, H. Zhou, H. Zhang, Y. Wang, Y. Gu, Carbon dots with intrinsic theranostic properties for bioimaging, red-lighttriggered photodynamic/photothermal simultaneous therapy in vitro and in vivo, Adv. Healthcare Mater. 5 (6) (2016) 665–675.
- [28] J. Liu, Y. Geng, D. Li, H. Yao, Z. Huo, Y. Li, K. Zhang, S. Zhu, H. Wei, W. Xu, Deep red emissive carbonized polymer dots with unprecedented narrow full width at half maximum, Adv. Mater. 32 (17) (2020) 1906641.
- [29] W. Li, Y. Liu, B. Wang, H. Song, Z. Liu, S. Lu, B. Yang, Kilogram-scale synthesis of carbon quantum dots for hydrogen evolution, sensing and bioimaging, Chin. Chem. Lett. 30 (12) (2019) 2323–2327.
- [30] M.K. Barman, A. Patra, Current status and prospects on chemical structure driven photoluminescence behaviour of carbon dots, J. Photochem. Photobiol., A C 37 (2018) 1–22.
- [31] L. Ai, Y. Yang, B. Wang, J. Chang, Z. Tang, B. Yang, S. Lu, Insights into photoluminescence mechanisms of carbon dots: advances and perspectives, Sci. Bull. 66 (8) (2021) 839–856.
- [32] H.A. Nguyen, I. Srivastava, D. Pan, M. Gruebele, Unraveling the fluorescence mechanism of carbon dots with sub-single-particle resolution, ACS Nano 14 (5) (2020) 6127–6137.
- [33] S. Zhu, Y. Song, X. Zhao, J. Shao, J. Zhang, B. Yang, The photoluminescence mechanism in carbon dots (graphene quantum dots, carbon nanodots, and polymer dots): current state and future perspective, Nano Res. 8 (2) (2015) 355–381.
- [34] A. Cayuela, M. Soriano, C. Carrillo-Carrión, M. Valcárcel, Semiconductor and carbon-based fluorescent nanodots: the need for consistency, Chem. Commun. 52 (7) (2016) 1311–1326.
- [35] L. Fang, M. Wu, C. Huang, Z. Liu, J. Liang, H. Zhang, Industrializable synthesis of narrow-dispersed carbon dots achieved by microwave-assisted selective carbonization of surfactants and their applications as fluorescent nano-additives, J. Mater. Chem. 8 (40) (2020) 21317–21326.
- [36] L. Li, Y. Li, Y. Ye, R. Guo, A. Wang, G. Zou, H. Hou, X. Ji, Kilogram-scale synthesis and functionalization of carbon dots for superior electrochemical potassium storage, ACS Nano 15 (4) (2021) 6872–6885.
- [37] X. Niu, T. Song, H. Xiong, Large scale synthesis of red emissive carbon dots powder by solid state reaction for fingerprint identification, Chin. Chem. Lett. 32 (6) (2021) 1953–1956.
- [38] J. Manioudakis, F. Victoria, C.A. Thompson, L. Brown, M. Movsum, R. Lucifero, R. Naccache, Effects of nitrogen-doping on the photophysical properties of carbon dots, J. Mater. Chem. C 7 (4) (2019) 853–862.
- [39] W. Liu, C. Li, Y. Ren, X. Sun, W. Pan, Y. Li, J. Wang, W. Wang, Carbon dots: surface engineering and applications, J. Mater. Chem. B 4 (35) (2016) 5772–5788.

- [40] S. Kim, S.W. Hwang, M.-K. Kim, D.Y. Shin, D.H. Shin, C.O. Kim, S.B. Yang, J.H. Park, E. Hwang, S.-H. Choi, Anomalous behaviors of visible luminescence from graphene quantum dots: interplay between size and shape, ACS Nano 6 (9) (2012) 8203–8208.
- [41] N. Soni, S. Singh, S. Sharma, G. Batra, K. Kaushik, C. Rao, N.C. Verma, B. Mondal, A. Yadav, C.K. Nandi, Absorption and emission of light in red emissive carbon nanodots, Chem. Sci. 12 (10) (2021) 3615–3626.
- [42] T.-B. Wei, B.-R. Yong, L.-R. Dang, Y.-M. Zhang, H. Yao, Q. Lin, A simple water-soluble phenazine dye for colorimetric/fluorogenic dual-mode detection and removal of Cu²⁺ in natural water and plant samples, Dyes Pigments 171 (2019) 107707.
- [43] X. Lai, Q. Ye, R. Wang, P. Wang, J.-B. Liu, o-Phenylenediamine as a reaction-based probe for the fluorescent detection of Ce (IV) ions, J. Chem. Res. 45 (1–2) (2021) 28–33.
- [44] B.-R. Yong, T.-B. Wei, W.-J. Qu, Q. Lin, Y.-M. Zhang, H. Yao, Highly selective and sensitive chemosensor based on 2, 3-diaminophenazine hydrochloride for the detection of cyanide in pure water and its application in plant seed samples, New J. Chem. 42 (18) (2018) 14766–14771.
- [45] Q. Zhang, R. Wang, B. Feng, X. Zhong, K.K. Ostrikov, Photoluminescence mechanism of carbon dots: triggering high-color-purity red fluorescence

- emission through edge amino protonation, Nat. Commun. 12 (1) (2021) 1–13. [46] S. Yang, W. Li, C. Ye, G. Wang, H. Tian, C. Zhu, P. He, G. Ding, X. Xie, Y. Liu, C3N—a 2D crystalline, hole-free, tunable-narrow-bandgap semiconductor with ferromagnetic properties, Adv. Mater. 29 (16) (2017) 1605625.
- [47] Y. Ru, L. Ai, T. Jia, X. Liu, S. Lu, Z. Tang, B. Yang, Recent advances in chiral carbonized polymer dots: from synthesis and properties to applications, Nano Taday 24 (2020) 100052
- carbonized polymer dots: from synthesis and properties to applications, Nano Today 34 (2020) 100953.

 [48] L. Sui, W. Jin, S. Li, D. Liu, Y. Jiang, A. Chen, H. Liu, Y. Shi, D. Ding, M. Jin, Ul-
- trafast carrier dynamics of carbon nanodots in different pH environments, Phys. Chem. Chem. Phys. 18 (5) (2016) 3838–3845.

 [49] S. Ghosh, A. Ghosh, G. Ghosh, K. Marjit, A. Patra, Deciphering the relaxation
- mechanism of red-emitting carbon dots using ultrafast spectroscopy and global target analysis, J. Phys. Chem. Lett. 12 (33) (2021) 8080–8087.
- [50] A. Sciortino, M. Gazzetto, M.L. Soriano, M. Cannas, S. Cárdenas, A. Cannizzo, F. Messina, Ultrafast spectroscopic investigation on fluorescent carbon nanodots: the role of passivation, Phys. Chem. Chem. Phys. 21 (30) (2019) 16459–16467.
- [51] V. Strauss, A. Kahnt, E.M. Zolnhofer, K. Meyer, H. Maid, C. Placht, W. Bauer, T.J. Nacken, W. Peukert, S.H. Etschel, Assigning electronic states in carbon nanodots, Adv. Funct. Mater. 26 (44) (2016) 7975–7985.